2011 American Control Conference
on O'Farrell Street, San Francisco, CA, USA
June 29 - July 01, 2011

Calculation of Lyapunov Exponents Using Radial Basis Function Networks for Stability Analysis of Nonlinear Control Systems

Yuming Sun, Xingzheng Wang, Qiong Wu and Nariman Sepheri

Abstract— **The concept of Lyapunov exponents is a powerful tool for analyzing the stability of nonlinear dynamic systems, especially when the mathematical models of the systems are available. However, for real world systems, such models are often unknown. Estimating Lyapunov exponents using a time series has the advantage in that no mathematical model is required. The downside lies in that the method is believed to be reliable only for estimating positive exponents, and to suffer from generating spurious exponents. In contrary, the model-based method is constructive and reliable for calculating both positive and non-positive exponents. The use of the system Jacobians is the key to the advantages of the model-based method. In this paper, a novel approach is proposed, where the system Jacobians are derived based on system approximation using the Radial Basis Function (RBF) network. The proposed method inherits the advantages of the model-based method, yet no mathematical model is required. Two case studies are presented to demonstrate the efficacy of the proposed method. We believe that the work can contribute to stability analysis of nonlinear systems of which the dynamics are either difficult to model due to complexities or unknown.**

I. INTRODUCTION

Lyapunov exponents measure the average divergence or convergence rate of nearby orbits of an attractor in the state space. This concept has been the subject of intensive research for diagnosing chaotic systems and revealing stability of complex nonlinear systems [1], [2], [3], [4]. Wolf and his collaborators [2] described the procedure for calculating the spectrum of Lyapunov exponents from systems of which the mathematical models are well developed. The method essentially takes advantage of information brought by the system Jacobian matrix. The Jacobian matrix can describe the amount of distortion of the flow, which is induced by a transformation in the neighborhood of a given point. Müller [5] extended Wolf's method to non-smooth dynamical systems, *i.e.*, systems modeled by the ordinary differential equations that contain non-differentiable terms. Overall, both of these model-based algorithms are constructive and reliable for calculating all positive, zero and negative exponents, provided that Jacobian matrices are available.

Explicit mathematical models are however not always available in practice. And even they are at hand, the derivation of system Jacobian matrices can sometimes be unfeasible because of difficulties in modelling systems. This limitation bolstered many efforts for estimating Lyapunov exponents based on a time series [2], [6]. The most attractive advantage of using a time series is that the data can often be measured experimentally. On the other hand, it is stated that the time-series-based methods for calculating Lyapunov exponents arose primarily for chaotic systems, and they are not reliable for calculating negative and zero exponents due to the inaccuracy induced by the local linear mapping [7]. Additionally, identifying those true exponents from the spurious ones generated when a time series is used remains challenging [8].

Motivated by the above facts, a new method is developed in this work. The proposed method takes the benefit of the time-series-based method in that no mathematical models are required. On the other hand, it inherits the advantages of the model-based algorithm, in that it is constructive and valid for estimating both positive and non-positive Lyapunov exponents. In the proposed method, the time series of each state of the dynamical system are assumed to be available, which can be obtained either from a mathematical model or measured from experiments. A Radial Basis Function (RBF) network is constructed to approximate the nonlinear system. Once the network trained properly, the sequence of neural model Jacobian matrices can be obtained by utilizing the structure information of the RBF network. And with these neural model Jacobians, the spectrum of Lyapunov exponents can be estimated by following Wolf's model-based algorithm.

To demonstrate the efficacy of the proposed method, two dynamic systems are studied in this work. The first case study relates to a standing biped balance system, which is represented by a two-link inverted pendulum with one additional rigid foot-link. The biped is assumed to move in the sagittal plane. The foot-link is required to be stationary but not fixed on the ground, which imposes several constraints on the system. A linear feedback control law is designed to hold the biped upright, minimize the control torques, meanwhile satisfy all the constraints. For stability analysis, an RBF network is constructed to approximate the enforced system. Lyapunov exponents are calculated both from actual system Jacobians and neural model Jacobians, which are found very close to each other. Comparison between the numerical values of Lyapunov exponents based on actual and neural Jacobians is also made for a servovalve-controlled hydraulic actuator. In this case, the displacement of the valve spool is provided as a control signal to drive the actuator to reach a pre-desired position.

Y. Sun , Q. Wu and N. Sepheri are with the Department of Mechanical and Manufacturing Engineering, University of Manitoba, Winnipeg, MB R3T5V6, Canada umsun82@cc.umanitoba.ca, cwu@cc.umanitoba.ca, nariman@cc.umanitoba.ca

X. Wang is with the XTech Inc., 2-16-1-1103 Kokubuminami, Ebina-shi, Kanagawa-ken, Japan wang_xp@xtech.co.jp

II. METHODOLOGY

A. Mathematic preliminary

Here we first review the concept of Lyapunov exponents, followed by a brief description of procedures of calculating Lyapunov exponents based on mathematical models.

1) The concept of Lyapunov exponents: Consider a smooth dynamical system in an n-dimensional state space expressed in the following form:

$$\dot{\boldsymbol{x}} = \boldsymbol{f}(\boldsymbol{x}, t), \tag{1}$$

where $\boldsymbol{x} \in \mathbb{R}^n$ is the state vector, $\boldsymbol{x}(0) = \boldsymbol{x}_0$, and $\boldsymbol{f}(\boldsymbol{x}, t)$ is a continuously differentiable vector function. Monitoring the long-term evolution of an infinitesimal n-sphere of initial conditions, the sphere becomes an n-ellipsoid due to the local deforming nature of the flow. The i^{th} dimensional Lyapunov exponent is then defined in terms of the length of the ellipsoidal principal axis $\|\delta x_i(t)\|$:

$$\lambda_i = \lim_{t\to\infty} \frac{1}{t} \ln \frac{\|\delta x_i(t)\|}{\|\delta x_i(t_0)\|}, \quad i = 1, \ldots, n, \tag{2}$$

where $\|\delta x_i(t_0)\|$ and $\|\delta x_i(t)\|$ represent the lengths of the i^{th} principal axis of the infinitesimal n-dimensional hyper-ellipsoid at initial and current time instances, t_0 and t respectively. This definition indicates that Lyapunov exponents are related to the expanding or contracting nature of different directions in the state space. Besides, Lyapunov exponents are independent of initial conditions within the same stability regions.

In practical application, the finite-time Lyapunov exponents are frequently used in the form:

$$\lambda_i = \frac{1}{t} \ln \frac{\|\delta x_i(t)\|}{\|\delta x_i(t_0)\|}, \quad i = 1, \ldots, n. \tag{3}$$

In the limit as $t \to \infty$, the finite-time Lyapunov exponents converge to the true Lyapunov exponents [9].

The signs of Lyapunov exponents indicate the asymptotic property of the dynamical system. Generally in a dissipative system, an attractor is defined to be chaotic if the spectrum of Lyapunov exponents contains at least one positive exponent. For non-chaotic attractors such as periodic or quasi-periodic ones, there are only zero and negative exponents, while those exponentially stable equilibrium points are characterized by all Lyapunov exponents being negative [3].

2) Calculation of model-based Lyapunov exponents: Wolf *et al.* [2] developed the algorithm for calculating the spectrum of Lyapunov exponents from explicit mathematical models of systems. In their work a "fiducial" trajectory (the center of the sphere) is defined by the action of the nonlinear motion equations on some initial condition. The principal axes are determined by the evolution via the linearized equations of an initially orthonormal vector frame anchored to the fiducial trajectory. This leads to the following set of equations [2]:

$$\dot{\boldsymbol{x}}(t) = \boldsymbol{f}\big(\boldsymbol{x}(t)\big), \tag{4a}$$

$$\dot{\boldsymbol{\Psi}}_t = \boldsymbol{J}\big(\boldsymbol{x}(t)\big)\boldsymbol{\Psi}_t, \tag{4b}$$

where $\boldsymbol{\Psi}_t$ is the state transition matrix of the linearized system $\delta\boldsymbol{x}(t) = \boldsymbol{\Psi}_t \delta\boldsymbol{x}(0)$. The Jacobian matrix $\boldsymbol{J}\big(\boldsymbol{x}(t)\big)$ is defined as

$$\boldsymbol{J}\big(\boldsymbol{x}(t)\big) = \left.\frac{\partial \boldsymbol{f}(\boldsymbol{x})}{\partial \boldsymbol{x}^{\mathrm{T}}}\right|_{\boldsymbol{x}=\boldsymbol{x}(t)}, \tag{5}$$

and the initial conditions for numerical integrations are $\begin{Bmatrix} \boldsymbol{x}(t_0) \\ \boldsymbol{\Psi}_t(t_0) \end{Bmatrix} = \begin{Bmatrix} \boldsymbol{x}_0 \\ \boldsymbol{I} \end{Bmatrix}$, where $\boldsymbol{I}$ is the identity matrix of proper dimension.

To avoid misalignment of all the vectors δx_i along the direction of maximal expansion, they are reorthonormalized at each integration step by involving the Gram-Schmidt Reorthonormalization (GSR) scheme, which generates an orthonormal set $\{u_1, \ldots, u_n\}$ of n vectors with the property that $\{u_1, \ldots, u_n\}$ spans the same subspace as $\{\delta x_1, \ldots, \delta x_n\}$. This orientation-preserving property of GSR suggests that the initial labeling of the vectors may be done arbitrarily. Once the orthonormal vector frame $\{u_1, \ldots, u_n\}$ is produced by GSR, for a large enough integer K, one can obtain Lyapunov exponents as follows with time-step size h properly chosen:

$$\lambda_i \approx \frac{1}{Kh} \sum_{j=1}^{K} \ln \|u_i^{(j)}\|, \quad i = 1, 2, \ldots, n, \tag{6}$$

where j is the number of integration steps.

B. Calculation of neural Jacobian-based Lyapunov exponents

Jacobian matrices are crucial in calculating Lyapunov exponents. In order to carry out stability analysis of systems with difficulties to obtain or model, system approximation based on time series is adopted in this work for determination of neural model Jacobians. It has been proven that any Borel measurable function can be approximated to any desired degree of accuracy by carefully choosing parameters of the network, provided the network structure is sufficiently large [10], [11].

The classical architecture of the RBF network is a three-layer feedforward network which contains the input layer, the hidden layer and the output layer. Fig. 1 shows a typical RBF network configuration with l hidden nodes. Such a

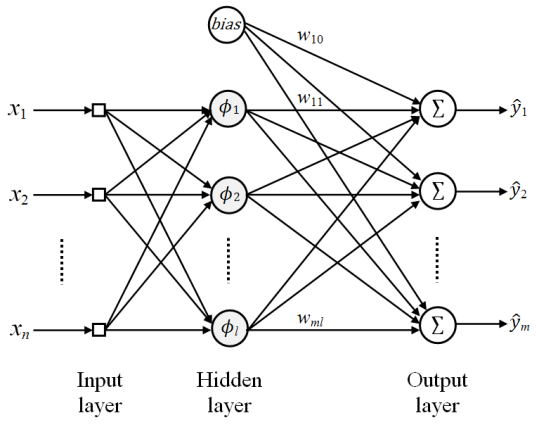

Fig. 1: A typical schematic of the RBF network.

network implements a mapping $f : \mathbb{R}^n \rightarrow \mathbb{R}^m$ according to the overall outputs:

$$\hat{y}_i = w_{i0} \times bias + \sum_{j=1}^{l} w_{ij}\phi_j(\|\boldsymbol{x} - \boldsymbol{c}_j\|), \quad i = 1, 2, \ldots, m, \tag{7}$$

where $\boldsymbol{x} \in \mathbb{R}^n$ is the input vector. w_{ij} are the output weights, and the first index of the weight indicates the destination unit of the weight, and the second one indicates the input source for that weight. The bias neuron always emits 1, and its connection weight w_{i0} has an effect of increasing or lowering the net input of the summation junction in the next layer, which facilitates training. $\phi_j(\cdot)$ is a given function with its center vector defined as $\boldsymbol{c}_j = [c_{j1}, c_{j2}, \ldots, c_{jn}]^{\mathrm{T}}$, where $1 \leq j \leq l$. In our study, we select the Gaussian function for ϕ_j, which has the following expression:

$$\phi_j = \exp(-\frac{\|\boldsymbol{x} - \boldsymbol{c}_j\|^2}{2\sigma_j^2}), \tag{8}$$

where σ_j is the width of the j^{th} Gaussian function.

To appropriately choose the parameters of the network, the centers of the RBF network $\boldsymbol{c}_j$ can be determined using the K-means clustering method, while the width σ_j can be fixed by employing the K-nearest neighbours heuristic typically [12] . For the output layer, the linear weights w_{ij} can be found by following the steps of gradient descent with momentum algorithm.

Once the RBF network is developed for an unknown multiple-input multiple-output (MIMO) system, the system Jacobian matrices can be obtained from the structure information of the network. Specifically, at step k, one entry of the Jacobian matrix, located at the m^{th} row and the n^{th} column can be written in the following form:

$$J_{mn}(k) = \frac{\partial y_m(k)}{\partial x_n(k)} \approx \frac{\partial \hat{y}_m(k)}{\partial x_n(k)} = \sum_{j=1}^{l} w_{mj}\phi_j \frac{c_{ji} - x_i(k)}{\sigma_j^2}. \tag{9}$$

Given the series of neural model Jacobians at different time instances, computing Lyapunov exponents based on time series, reduces to the problem of calculating exponents from an explicit mathematic expression, which is a substitute for the system under study. Since the RBF network can approximate the actual dynamical system within an arbitrary accuracy, its Jacobian matrices should be capable of reflecting the actual system Jabians precisely.

III. CASE STUDIES

A. Case study I: bipedal balance system

Fig. 2(A) shows a standing biped robot, which is simplified as a two-link inverted pendulum system representing the leg and the torso respectively with one rigid foot-link. The joints 1 and 2 can be considered as the ankle and hip joints, and the foot-link provides a base of support on the ground. The free body diagram of the two-link inverted pendulum and the free body diagram of the foot-link are shown in Figs. 2(B) and 2(C) respectively. The biped is assumed to move in the sagittal plane and the foot-link is required to be stationary, which leads constraints between the foot link and the ground. The control torques are applied at both joints to maintain the biped at the upright posture and to satisfy the constraints during standing. The model parameters are listed in Table I.

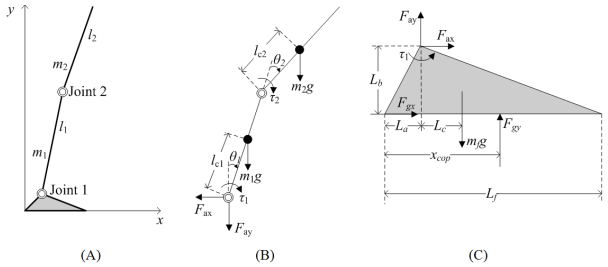

Fig. 2: (A) the simplified biped model, (B) the free body diagram of the two-link inverted pendulum, and (C) the free body diagram of the foot-link.

In Fig. 2, $\boldsymbol{\theta} = [\theta_1, \theta_2]^{\mathrm{T}}$ are the two joint angles (clockwise as "+"), $\boldsymbol{\tau} = [\tau_1, \tau_2]^{\mathrm{T}}$ are control torques applied at both joints (clockwise as "+"). Defining $\boldsymbol{q} = [q_1, q_2, q_3, q_4]^{\mathrm{T}} = [\theta_1, \theta_2, \dot{\theta}_1, \dot{\theta}_2]^{\mathrm{T}}$. According to the Euler-Lagrangian formulation, the state-space model of the biped balance system can be written in the following form:

$$\begin{cases} \dot{q}_1 = q_3, \\ \dot{q}_2 = q_4, \\ \dot{q}_3 = \Big(\delta\tau_1 - (\delta + \frac{\beta}{2}\cos q_2)\tau_2 + \frac{\beta}{2}\sin q_2\big(\delta q_4(q_3 + q_4) \\ \quad -\frac{\beta}{2}q_3q_4\cos q_2\big) + \Big(\delta(m_1l_{c1} + m_2l_1)\sin q_1 - \frac{\beta}{2} \\ \quad \times m_2l_{c2}\cos q_2\sin(q_1 + q_2)\Big)g\Big)/D, \\ \dot{q}_4 = \Big(-(\delta + \frac{\beta}{2}\cos q_2)\tau_1 + (\alpha + \beta\cos q_2)\tau_2 + \frac{\beta}{2}\sin q_2 \\ \quad \times q_4\Big(q_3(\alpha - 2\delta) - q_4(\delta + \frac{\beta}{2}\cos q_2)\Big) + \Big((\alpha - \delta \\ \quad + \frac{\beta}{2}\cos q_2)m_2l_{c2}\sin(q_1 + q_2) - (\delta + \frac{\beta}{2}\cos q_2) \\ \quad \times (m_1l_{c1} + m_2l_1)\sin q_1\Big)g\Big)/D. \end{cases} \tag{10}$$

where $\alpha = m_1l_{c1}^2 + m_2l_1^2 + m_2l_{c2}^2 + I_1 + I_2$, $\beta = 2m_2l_1l_{c2}$, $\delta = m_2l_{c2}^2 + I_2$. D is the determinant of the matrix $\begin{bmatrix} \alpha + \beta\cos\theta_2 & \delta + \frac{\beta}{2}\cos\theta_2 \\ \delta + \frac{\beta}{2}\cos\theta_2 & \delta \end{bmatrix}$. Moreover, the horizontal and vertical ground reaction forces can be derived as:

$$F_{gx} = m_1a_{x_1} + m_2a_{x_2}, \tag{11a}$$

$$F_{gy} = m_1a_{y_1} + m_2a_{y_2} + (m_1 + m_2 + m_f)g, \tag{11b}$$

where

$$\begin{aligned} a_{x_1} &= -l_{c1}\sin\theta_1\dot{\theta}_1^2 + l_{c1}\cos\theta_1\ddot{\theta}_1, \\ a_{x_2} &= -l_1\sin\theta_1\dot{\theta}_1^2 + l_1\cos\theta_1\ddot{\theta}_1 - l_{c2}\sin(\theta_1 + \theta_2)(\dot{\theta}_1 + \dot{\theta}_2)^2 \\ &\quad + l_{c2}\cos(\theta_1 + \theta_2)(\ddot{\theta}_1 + \ddot{\theta}_2), \\ a_{y_1} &= -l_{c1}\cos\theta_1\dot{\theta}_1^2 - l_{c1}\sin\theta_1\ddot{\theta}_1, \\ a_{y_2} &= -l_1\cos\theta_1\dot{\theta}_1^2 - l_1\sin\theta_1\ddot{\theta}_1 - l_{c2}\cos(\theta_1 + \theta_2)(\dot{\theta}_1 + \dot{\theta}_2)^2 \\ &\quad - l_{c2}\sin(\theta_1 + \theta_2)(\ddot{\theta}_1 + \ddot{\theta}_2). \end{aligned}$$

Since the foot link is assumed to be still, but not fixed on the ground, there is a set of constraints imposed on the system. The gravity constraint $F_{gy} > 0$ guarantees

TABLE I: Biped model parameters.

Symbols	Parameters	Nominal Value
m_1	mass of the link 1	48.720 [kg]
m_2	mass of the link 2	28.960 [kg]
m_f	mass of the foot link	2.320 [kg]
l_1	length of the link 1	0.998 [m]
l_2	length of the link 2	0.712 [m]
l_{c1}	location of mass center of the link 1	0.499 [m]
l_{c2}	location of mass center of the link 2	0.356 [m]
I_1	inertia of the link 1	4.044 [kg·m^2]
I_2	inertia of the link 2	1.223 [kg·m^2]
L_f	length of the foot link	0.270 [m]
L_a	horizontal distance between the ankle and the heel	0.050 [m]
L_b	ankle height	0.070 [m]
L_c	horizontal distance between the mass center of the foot and the ankle	0.085 [m]
g	gravity acceleration	9.8 [m/s^2]
μ	friction constant	0.5
x_{cop}	location of the center of pressure (COP)	

the biped's foot will not lift from the ground; the friction constraint $|F_{gx}| \leq \mu F_{gy}$ ensures the biped's foot will not slide on the ground; and the COP constraint $0 \leq x_{cop} \leq L_f$ along with $x_{cop} = L_a - \frac{L_b F_{gx} + \tau_1 - L_c m_f g}{F_{gy}}$ promises the COP will always reside within the boundary of support, i.e., there is no rolling of the foot-link about either the toe or the heel. These constraints determine the bounds on the control torques, which change with the states of the system [13]. However, owing to the high nonlinearity of this two-link biped model, the analytical expression of the control bounds cannot be obtained in terms of $\boldsymbol{\theta}$, $\dot{\boldsymbol{\theta}}$ and $\ddot{\boldsymbol{\theta}}$. Thus here we only monitor the evolutions of F_{gx}, F_{gy} and the location of pressure center x_{cop}. The control torques and the simulation will be terminated if any of these three constraints is violated. This is different from most previous papers [14], [15], where the constraints between the bipedal feet and the ground are assumed to be satisfied automatically.

A classical state feedback control law via linear-quadratic regulator (LQR) algorithm is adopted in this case for stabilizing the standing biped and meanwhile minimizing a predefined quadratic cost index $J = \frac{1}{2}\int_0^\infty (\boldsymbol{x}^{\mathrm{T}}\boldsymbol{Q}\boldsymbol{x} + \boldsymbol{u}^{\mathrm{T}}\boldsymbol{R}\boldsymbol{u})dt$. The weight matrix $\boldsymbol{Q} = \mathrm{diag}(\boldsymbol{Q}_1, \boldsymbol{Q}_2)$ with $\boldsymbol{Q}_1 = \boldsymbol{Q}_2 = \begin{bmatrix} 1000 & -500 \\ -500 & 1000 \end{bmatrix}$, $\boldsymbol{R} = \mathrm{diag}(1000, 10000)$. The system (10) is linearized first about the equilibrium point ($\boldsymbol{q} = [0, 0, 0, 0]^{\mathrm{T}}$). And the state feedback gain $\boldsymbol{F}$ is found to be $\begin{bmatrix} 1061.5 & 63.5 & 345.3 & 53.9 \\ 273.3 & 206.3 & 106.5 & 43.8 \end{bmatrix}$.

The system initial condition is given by $\boldsymbol{q} = [-0.05\mathrm{rad}, 0.03\mathrm{rad}, 0.05\mathrm{rad/s}, -0.03\mathrm{rad/s}]^{\mathrm{T}}$. Figs. 3 to 4 show the simulation results of the controlled biped. The evolution of the states and control torques displayed in Fig. 3 indicates that the biped can be driven successfully to the upright posture within 2.5 seconds. Figs. 4(A) and 4(B) demonstrate time history versus F_{gy} and F_{gx} respectively. The positive vertical ground reaction force F_{gy} implies the support foot is always in contact with the ground. And the horizontal ground reaction force F_{gx} can be observed residing in the bounds of the static friction ($[-\mu F_{gy}, \mu F_{gy}]$), indicating the foot-link does not slip. The location of the center of pressure (x_{cop}) staying within the contact surface is shown in Fig. 4(C).

The proposed control strategy for system (10) is designed through the linearized system, there is no guarantee that it works well when implemented on the nonlinear system. Due to complexity of the original nonlinear system, Lyapunov exponents are employed to analyze the stability of the controlled biped balance system. For system approximation, an RBF network is constructed. We define a sampling time sequence $\{t_k\}_{k=0}^f$, and use $[\boldsymbol{q}(t_0), \cdots, \boldsymbol{q}(t_f)]$ as the input of the neural model, $[\dot{\boldsymbol{q}}(t_0), \cdots, \dot{\boldsymbol{q}}(t_f)]$ as the desired output. Table II summarizes the RBF network for the biped balance system.

Since the system is 4-dimensinal, totally there are 16 entries in the Jacobian matrix. Our numerical results show that all the absolute errors between the elements of the actual system Jacobians and the neural model Jacobians become

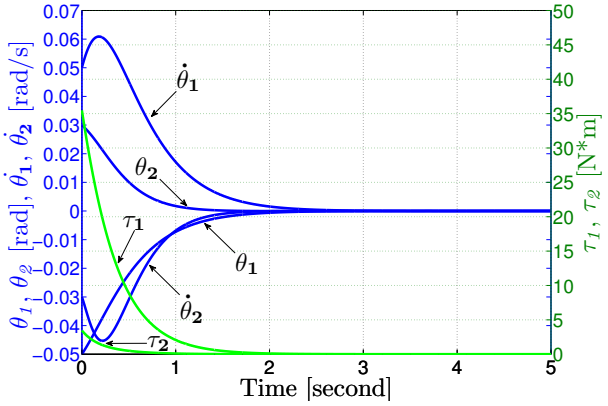

Fig. 3: Evolution of the states and control torques, where the left y-axis is for measuring system states and the right y-axis is for scaling the magnitude of two control torques.

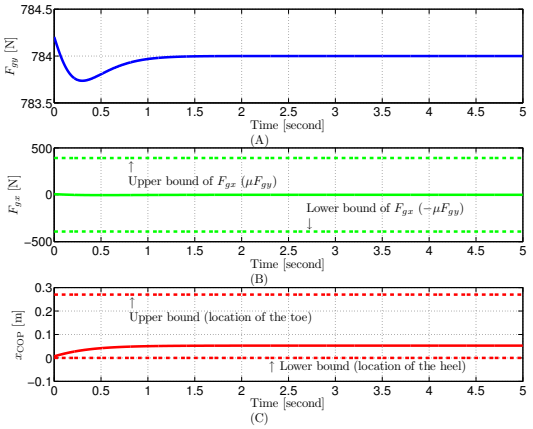

Fig. 4: Evolution of (A) F_{gy}, (B) F_{gx} and (C) x_{cop}.

TABLE II: Structure of the RBF network for the biped balance system.

Number of hidden nodes	10
Number of inputs, outputs	4, 4
Number of clustering samples	3000
Mean-squared error after training	1.870e-12

constant after the biped is stabilized at the upright posture, the errors stay within the range $(-0.03, 0.02)$, implying that our RBF model is accurate enough to approximate the controlled biped system. Additionally, all four Lyapunov exponents in 100 seconds are displayed in Fig. 5, where the solid lines represent the evolution of Lyapunov exponents based on the actual system Jacobians, being compared with the dashed lines representing those from the neural model Jacobians. And all Lyapunov exponents converge to negative constants which are listed in Table III, indicating that the bipedal balance system is exponentially stable about the equilibrium point. The low relative errors demonstrate that the proposed method of deriving Jacobians from the RBF network is effective for the calculation of Lyapunov exponents.

B. Case study II: hydraulic actuator system

In practice the rates of the system states are often unavailable or difficult to measure. Thus, it is desirable to monitor the system states rather than rates of the states under such conditions. A servovalve-controlled hydraulic actuator system of which schematic shown in Fig. 6 is studied here. The system is composed of a double-ended horizontal hydraulic actuator heading towards the desired position, $x_d = 0.01$m. All the system parameters are taken from [16]. And the basic state equations describing the servovalve-actuator dynamics

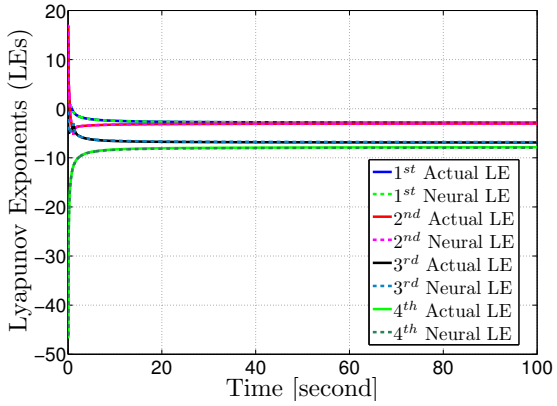

Fig. 5: Evolution of the Lyapunov exponents.

TABLE III: Lyapunov exponents (LEs) and their relative errors (REs) after 100 seconds.

LEs	Mathematical Model	Neural Model	REs
1^{st} LE	-2.8699	-2.8700	0.003%
2^{nd} LE	-2.9933	-2.9929	0.01%
3^{rd} LE	-7.1580	-7.2845	1.77%
4^{th} LE	-7.5334	-7.3829	2.00%

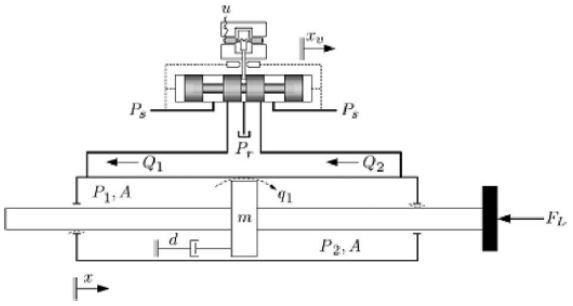

Fig. 6: Schematic of a typical valve-controlled hydraulic actuator.

can be formed as:

$$\begin{cases} \dot{x}_p = v_p, \\ \dot{v}_p = \frac{1}{m}(AP_L - bv_p - F_L), \\ \dot{P}_L = \frac{4\beta}{V}(C_v w x_v \sqrt{\frac{P_s - \text{sgn}(x_v)P_L}{\rho}} - Av_p). \end{cases} \tag{12}$$

Referring to system (12), the system states are actuator position x_p, actuator velocity v_p, load pressure $P_L = P_1 - P_2$. F_L denotes an external (environmental) force, which is proportional to x_p. The valve spool displacement, $x_v = k_p(x_d - x_p)$, serves as a control signal here and $k_p = 0.003$. The term 'sgn(x_v)' denotes the sign function of x_v, which is used to account for the directionality of the valve spool.

One can get the equilibrium point of system (12) as $[x_d \;\; 0 \;\; \frac{kx_d}{A}]^{\text{T}}$. Define a new state vector $\tilde{\boldsymbol{x}} = [\tilde{x} \;\; \tilde{v} \;\; \tilde{P}]^{\text{T}} = [x_p - x_d \;\; v_p \;\; P_L - \frac{kx_d}{A}]^{\text{T}}$, then system (12) can be transferred into the following form with the new equilibrium point located at the origin:

$$\begin{cases} \dot{\tilde{x}} = \tilde{v}, \\ \dot{\tilde{v}} = \frac{1}{m}(A\tilde{P} - b\tilde{v} - k\tilde{x}), \\ \dot{\tilde{P}} = -\frac{4\beta}{V}\left(C_v w k_p \tilde{x} \sqrt{\frac{P_s + k_p \text{sgn}(\tilde{x})(\tilde{P} + \frac{kx_d}{A})}{\rho}} + A\tilde{v}\right). \end{cases} \tag{13}$$

With setting the initial state $\tilde{\boldsymbol{x}} = [-0.01\text{m} \;\; 0\text{m/s} \;\; -1.18\text{MPa}]^{\text{T}}$, system (13) is first regulated for guiding the states to the fixed point. The system trajectory and the evolution of the control signal is shown in Fig. 7, from which

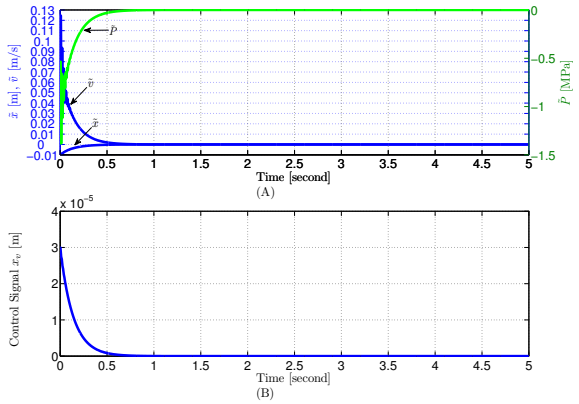

Fig. 7: Evolution of (A) the states of the hydraulic actuator system, where the left y-axis is for measuring $\tilde{x}$ and $\tilde{v}$ while the right y-axis is for measuring $\tilde{P}$; (B) the control signal x_v.

it can be seen all the states are quickly driven to zero.

An RBF network is established as well to approximate the dynamics of the discretized mathematical model. Different from the previous case, here the desired output of the network is setted to $[\tilde{\boldsymbol{x}}(t_1), \cdots, \tilde{\boldsymbol{x}}(t_f)]$, while the input is $[\tilde{\boldsymbol{x}}(t_0), \cdots, \tilde{\boldsymbol{x}}(t_f - 1)]$. Table IV provides the summary of the trained RBF network.

Since the established RBF network is an approximator of discretized continuous system (13) based on the Runge-Kutta method, the numerical values of these neural model Jacobians are incomparable with the Jacobians of the original continuous system. However, Lyapunov exponents calculated from the RBF network are very close to the actual exponents derived from mathematical model. Fig. 8 illustrates the evolution of all three exponents of system (13) in 100 seconds, where the solid lines stand for the exponents derived from the actual system, while those dashed lines correspond to the ones obtained from neural model. All the negative constants to which the system exponents converge are shown in Table V, indicating the system is exponentially stable. The average relative error of all three exponents is 1.88%, which demonstrates the effectiveness of the method proposed in this work.

IV. CONCLUSIONS

A novel method for computing Lyapunov exponents has been developed in this paper on the basis of the RBF network. The method is advanced in that (1) no mathematical models are required, (2) derivation of Jacobian matrices is straightforward, and (3) all Lyapunov exponents, regardless of the signs, can be estimated reliably. Two case studies have been employed to demonstrate the efficacy of our developed method. The accuracy of Lyapunov exponents calculated based on the neural model Jacobians from both case studies are extremely high.

One major limitation of this work is that we assume the exact system dimensionality is known and all states histories are available for system approximation. However in some cases only information of parts of states are available. Hence, a further study on the computation of Lyapunov exponents based on time series of some of the states or even a scalar time series through system identification using the RBF network [17], is highly desirable.

TABLE IV: Structure of the RBF network for the hydraulic actuator system.

Number of hidden nodes	100
Number of inputs, outputs	3, 3
Number of clustering samples	2500
Mean-squared error after training	1.0310e-12

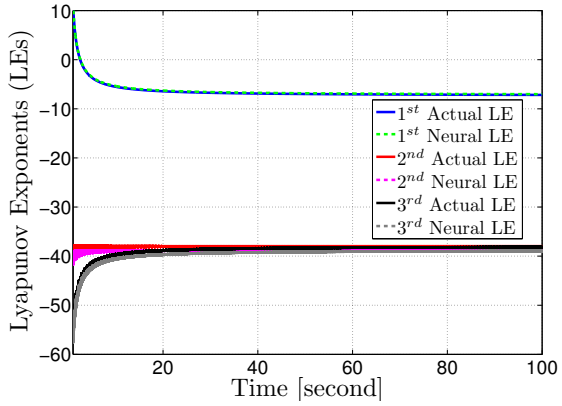

Fig. 8: Evolution of the Lyapunov exponents.

TABLE V: Lyapunov exponents (LEs) and their relative errors (REs) after 100 seconds.

LEs	Mathematical Model	Neural Model	REs
1^{st} LE	-7.1693	-6.9701	2.78%
2^{nd} LE	-37.9826	-38.5416	1.47%
3^{rd} LE	-38.1660	-38.7008	1.40%

REFERENCES

[1] V. I. Oseledec, "A multiplicative ergodic theorem: Lyapunov characteristic numbers for dynamical system," *Transactions of the Moscow Mathematical Society*, vol. 19, pp. 197–231, 1968.

[2] A. Wolf, J. B. Swift, H. L. Swinney, and J. A. Vastano, "Determining lyapunov exponents from a time series," *Physics D*, vol. 16, pp. 285–317, 1985.

[3] G. P. Williams, *Chaos Theory Tamed*. Washington D C: Joseph Henry Press, 1997.

[4] W. Kinsner, "Characterizing chaos through lyapunov metrics," *IEEE Transactions on Systems, Man and Cybernetics. Part C, Applications and Reviews*, vol. 36, no. 2, pp. 141–151, 2006.

[5] P. C. Müller, "Calculation of lyapunov exponents for dynamic systems with discontinuities," *Chaos, Solitons Fractals*, vol. 5, no. 9, pp. 1671–1681, 1995.

[6] M. Sano and Y. Sawada, "Measurement of the lyapunov exponents spectrum from chaotic time series," *Physical Review Letters*, vol. 55, pp. 1082–1085, June 1985.

[7] R. Brown, P. Bryant, and H. D. I. Abarbanel, "Computing the lyapunov spectrum of a dynamical system from an observed time series," *Physical Review A*, vol. 43, pp. 2787–2806, March 1991.

[8] C. Yang and Q. Wu, "On stability analysis via lyapunov exponents calculated from a time series using nonlinear mapping - a case study," *Nonlinear Dynamics*, vol. 59, pp. 239–257, 2010.

[9] X. Zeng, R. A. Pielke, and R. Eykholt, "Extracting lyapunov exponents from short time series of low precision," *Modern Physics Letters B*, vol. 6, no. 2, pp. 55–75, 1992.

[10] J. Park and I. W. Sandberg, "Universal approximation using radial-basis-function networks," *Neural Computation*, vol. 3, pp. 246–257, June 1991.

[11] K. Funahashi, "On the approximate realization of continuous mappings by neural networks," *Neural Networks*, vol. 2, no. 3, pp. 183–192, 1989.

[12] K. B. Kim, J. B. Park, Y. H. Choi, and G. Chen, "Control of chaotic dynamical systems using radial basis function network approximators," *Information Sciences*, vol. 130, pp. 165–183, December 2000.

[13] C. Yang and Q. Wu, "Effects of constraints on bipedal balance control," in *American Control Conference*, (Minneapolis, USA), pp. 2510–2515, 2006.

[14] Z. Liu and C. Li, "Fuzzy neural networks quadratic stabilization output feedback control for biped robots via h infiniti approach," *IEEE Transactions On Systems, Man, And Cybernetics—Part B: Cybernetics*, vol. 33, pp. 67–84, Jan 2003.

[15] X. Mu and Q. Wu, "Development of a complete dynamic model of a planar five-link biped and sliding mode control of its locomotion during the double support phase," *International Journal of Control*, vol. 77, pp. 789–799, May 2004.

[16] M. Karpenko and N. Sepehri, "Fault-tolerant control of a servohydraulic positioning system with crossport leakage," *IEEE Transactions on Control Systems Technology*, vol. 13, pp. 155–161, Jan 2005.

[17] S. Haykin, *Neural Networks: A Comprehensive Foundation*. New Jersey: Prentice Hall, 2nd ed., 1999.